

UC Irvine

Faculty Publications

Title

Variability in the location of the Antarctic Polar Front (90°-20°W) from satellite sea surface temperature data

Permalink

<https://escholarship.org/uc/item/9989q7rb>

Journal

Journal of Geophysical Research, 102(C13)

ISSN

0148-0227

Authors

Moore, J. Keith
Abbott, Mark R
Richman, James G

Publication Date

1997

DOI

10.1029/97JC01705

Copyright Information

This work is made available under the terms of a Creative Commons Attribution License, available at <https://creativecommons.org/licenses/by/4.0/>

Peer reviewed

Variability in the location of the Antarctic Polar Front (90°–20°W) from satellite sea surface temperature data

J. Keith Moore, Mark R. Abbott, and James G. Richman

College of Oceanic and Atmospheric Sciences, Oregon State University, Corvallis

Abstract. The path of the Antarctic Polar Front (PF) is mapped using satellite sea surface temperature data from the NOAA/NASA Pathfinder program. The mean path and variability of the PF are strongly influenced by bathymetry. Meandering intensity is weaker where the bathymetry is steeply sloped and increases in areas where the bottom is relatively flat. There is an inverse relationship between meandering intensity and both the width of the front and the change in temperature across it. There is a persistent, large separation between the surface and subsurface expressions of the PF at Ewing Bank on the Falkland Plateau.

1. Introduction

The Antarctic Polar Front (PF) is a strong jet within the Antarctic Circumpolar Current (ACC), which flows eastward continuously around Antarctica [Nowlin and Klinck, 1986]. The PF, also known as the Antarctic Convergence, is the location where Antarctic surface waters moving to the north sink rapidly below Subantarctic waters [Deacon, 1933, 1937]. Thus the PF is a region of elevated current speeds and strong horizontal gradients in density, temperature, salinity, and other oceanographic properties. The PF marks an important boundary in terms of air-sea fluxes and the heat and salt budgets of the Southern Ocean. The path of the PF exhibits considerable variability in the form of mesoscale meandering, eddies, and ring formation [Mackintosh, 1946; Joyce *et al.*, 1978]. The region lying north of the PF and south of the Subantarctic Front (SAF) is termed the Polar Frontal Zone (PFZ).

The PF has both surface and subsurface expressions, whose locations do not necessarily coincide. Strong gradients in sea surface temperature mark the surface expression [Deacon, 1933, 1937; Mackintosh, 1946]. Subsurface definitions for the PF mark the location where Antarctic surface waters descend rapidly, such as the point where the minimum potential temperature layer sinks below 200 m depth [Deacon, 1933, 1937; Orsi *et al.*, 1995]. South of Africa, the subsurface and surface expressions of the PF are typically separated by distances less than ~50 km, although separations up to 300 km have been noted [Lutjeharms and Valentine, 1984; Lutjeharms, 1985]. Sparrow *et al.* [1996] concluded that there is a wide separation between the surface and subsurface PF expressions in the vicinity of the Kerguelen Plateau. Deacon [1933] and Guretskii [1987] noted that in some regions of the southwest Atlantic, Subantarctic surface waters extend southward over the cold Antarctic surface layer, placing the PF surface expression south of the subsurface expression. These southward extensions of Subantarctic waters occurred only in a relatively thin surface layer (~100 m deep [Deacon, 1933]).

We have used the strong sea surface temperature (SST) gradient at the PF to map its surface expression in the region 90°–20°W over the 2 year period 1987–1988. Similar mapping

Copyright 1997 by the American Geophysical Union.

Paper number 97JC01705.
0148-0227/97/97JC-01705\$09.00

of meandering jets and fronts has been done previously for the PF [Legeckis, 1977] and other strong frontal systems [Hansen and Maul, 1970; Olson *et al.*, 1983; Cornillon, 1986].

Satellite altimeter data has shown that there is little zonal coherence in the variability of the ACC [Fu and Chelton, 1984; Sandwell and Zhang, 1989; Chelton *et al.*, 1990; Gille, 1994; Gille and Kelly, 1996]. These studies emphasize the importance of local and regional instabilities [Chelton *et al.*, 1990; Gille and Kelly, 1996]. Gille [1994] used Geosat altimeter data and a meandering jet model to map the mean location of the PF and the SAF. The large changes in sea surface height detected by the two-jet model would likely be associated with the subsurface expression of the PF [Gille, 1994]. Thus comparison of our results with those based on altimeters [Gille, 1994] as well as in situ subsurface data [Orsi *et al.*, 1995] can provide insights into relationships between the surface and subsurface expressions of the PF.

Barotropic flow in the oceans over smoothly varying topography tends to conserve angular momentum by following lines of constant potential vorticity $(f + \zeta)/H$, where f is the planetary vorticity, ζ is relative vorticity, and H is ocean depth. In open ocean areas the planetary vorticity is much larger than the relative vorticity, and mean potential vorticity can be approximated as f/H . We will use the term planetary potential vorticity for this f/H approximation. We compare the path of the Polar Front with the planetary potential vorticity field.

In the Southern Ocean the large changes in ocean depth associated with the mid-ocean ridges and Drake Passage do not permit the ACC to follow lines of constant planetary potential vorticity circumglobally [Koblinsky, 1990]. The ACC is forced at Drake Passage and the north Scotia Ridge across isolines of planetary potential vorticity, causing inputs of relative vorticity to the water column through the shrinking of vortex lines. This relative vorticity is likely dissipated through nonlinear processes such as eddy action or Rossby waves.

2. Materials and Methods

The position of the Antarctic Polar Front was mapped using satellite SST data from 1987–1988. The satellite data were the daily equal-angle “best SST” files (9 km spatial resolution) of the NOAA/NASA Pathfinder program. The Pathfinder program data set has high-resolution global SST coverage derived from the advanced very high resolution radiometer (AVHRR)

aboard the NOAA Polar Orbiters [Brown *et al.*, 1993]. The Pathfinder data have better coverage in high latitude, persistently cloudy regions than previously available satellite SST [Smith *et al.*, 1996].

Cloud cover is particularly persistent over the Southern Ocean [Legeckis, 1977; Bishop and Rossow, 1991], which limited our temporal resolution. In order to minimize gaps in the data due to cloud cover, daily files were composite averaged into weekly files using all available data (including ascending and descending satellite passes). The resulting weekly images still had considerable gaps due to cloud cover, but at least portions of the PF were unobscured in each image.

The strong SST gradient at the PF was used to map its location. Images showing only the strong SST gradients were derived from the weekly SST maps. We defined a strong gradient as a temperature change $\geq 1.35^\circ\text{C}$ across a distance of ~ 45 km (pixel width varies with latitude). For each pixel in the weekly image a nine- by five-pixel box centered on that pixel was examined for strong temperature gradients in four directions (N-S, E-W, SW-NE, and SE-NW). The nine- by five-pixel dimensions were chosen so the distance across the box (N-S and E-W) was ~ 45 km. The distance across the box in the SW-NE and SE-NW directions at 55°S would be ~ 65 km.

If a strong temperature gradient ($\Delta T \geq 1.35^\circ\text{C}$) was detected in any of the four directions, the center pixel (with its SST value) was retained in the gradient map, otherwise it was set to zero (missing). Thus the gradient maps were subsets of the weekly temperature maps.

By experiment, we determined that the nine- by five-pixel box, with a $\Delta T \geq 1.35^\circ\text{C}$, was best at retaining the mesoscale features that we wished to map with an acceptable amount of noise (pixels retained which are not associated with the major fronts). The temperature resolution of the Pathfinder data is 0.15°C ; thus choices for ΔT were restricted to multiples of this value. If the ΔT value is set too low, noise overwhelms the front signal. If the ΔT value is too high, large portions of the front are not retained in the gradient maps. In the rare case ($< \sim 1\%$ of strong gradient pixels) where a strong gradient was detected but the center pixel was a missing data point, the temperature value for the center pixel was linearly interpolated from the two endpoints of the gradient.

Examples of the weekly temperature and gradient maps (from the first week of 1987) are shown in Plate 1. The nearly continuous area of strong gradient stretching from SW to NE across the Scotia Sea is the surface expression of the PF. Also visible to the north are regions of strong temperature gradient associated with the SAF. A warm core ring, pinched off from the PF, is also visible at $\sim 51^\circ\text{W}$, 56°S .

The location of the poleward edge of the PF was subjectively digitized by examining the weekly temperature and gradient maps. No path was mapped in areas where the front was not clearly visible. The poleward edge of the front marks the boundary between the PFZ and the northernmost extent of Antarctic surface waters. Satellite mapping studies of the Gulf Stream have also typically marked the poleward edge of the front [Cornillon, 1986].

The mean path of the PF was determined by first constructing a reference path (a subjective estimate of the mean path) and then calculating the mean deviation of all paths at right angles to this reference path. This mean deviation from the reference path defined the mean path. The computed mean path was smoothed with a five-point moving average in latitude and longitude. To quantify variability in the path of the PF, the

spatial displacement of individual paths at right angles from the mean path was calculated.

We tried several methods to quantify the SST gradient across the Polar Front; all of which gave similar results. Therefore we present only one method here. To quantify the temperature gradient across the front, we began at the poleward edge of the PF and moved up the temperature gradient until SST did not increase over a three-pixel (~ 20 – 30 km) distance or until a missing pixel was reached. The same method was used to measure the width of the front. Only complete transects were used to calculate the mean ΔT and distance across the PF.

A high-resolution predicted seafloor topography, derived from ship and Geosat altimeter data [Smith and Sandwell, 1994], was used to create maps of planetary potential vorticity for comparison with the PF paths. The predicted topography had a grid spacing of 3 arc min of longitude by 1.5 arc min of latitude. The predicted topography was also used to calculate the slope of the ocean floor across the PF (45 km to either side) and the mean depth along a swath 45 km north and south of the mean PF path.

3. Results and Discussion

All paths of the Antarctic Polar Front mapped during the years 1987–1988 are shown in Figure 1. Variability in the position of the PF has a relative minimum in three regions: at Drake Passage ($\sim 62^\circ$ – 57°W), between $\sim 78^\circ$ and 76°W , and along the eastern end of the Falkland Plateau (43° – 40°W). Variability increases west of $\sim 82^\circ\text{W}$, east of $\sim 33^\circ\text{W}$, and in the northern Scotia Sea between $\sim 50^\circ$ and 40°W .

The region of high variability in the northern Scotia Sea exhibited considerable meandering and ring formation, such that a clear path for the PF could not be distinguished at times even under cloud-free conditions. Gordon *et al.* [1977] reported that the PF was highly meandering in this region. Satellite altimeter studies have also found elevated mesoscale variability here [Sandwell and Zhang, 1989; Chelton *et al.*, 1990]. Relatively high levels of eddy kinetic energy have also been reported here from free-drifting buoy data [Daniault and Ménard, 1985; Johnson, 1989]. Relatively few paths were marked east of 25°W . This was not a function of cloud cover and seemed to be the result of a weakening of the SST gradient, such that it was often difficult to distinguish the PF from background “noise.”

The mean path of the Polar Front (1987–1988) through this region is displayed in Figure 2 (solid line). Our mean latitude of 58.7°S for the PF along 64°W agrees well with its subsurface position during the International Southern Ocean Studies (ISOS) Drake 79 experiment, where it ranged between $\sim 58.5^\circ$ and 59.5°S [Hofmann and Whitworth, 1985]. Ikeda *et al.* [1989] place the PF at 56.40°S along $\sim 54^\circ\text{W}$ during a cruise on March 12–20, 1987. Our latitude for the PF along 54°W for the 2 weeks which overlap this time period was 56.5°S .

It can be seen in Figures 1 and 2 that the PF often undergoes an S-shaped bend in the northern Scotia Sea (a feature described by Deacon [1933, 1937] and Mackintosh [1946]). Despite extensive meandering, the PF nearly always crosses the north Scotia Ridge at Shag Rock Passage [see Peterson and Whitworth, 1989] (Figures 1 and 2). This gap is the only area on the north Scotia Ridge with depths > 2000 m.

Also shown in Figure 2 are the mean paths for the Antarctic Polar Front reproduced from Gille [1994] and Orsi *et al.* [1995].

Note that these PF paths are based on three different mapping methods and three different definitions of the Polar Front. The subsurface temperature structure definition of *Orsi et al.* [1995] and the change in sea surface height definition used by *Gille* [1994] mark the subsurface expression of the PF, while our path reflects the surface expression.

The three PF paths are in relatively close agreement in several regions, including Drake Passage and just to the east ($\sim 65^\circ$ – 52° W), although *Gille* [1994] has a large poleward meander at $\sim 55^\circ$ W. In all three paths the PF turns southward just east of 40° W and again at $\sim 28^\circ$ W, where it encounters the Islas Orcadas Rise. Note that while our mean path turns southward, the PF sometimes crosses or flows north of the Islas Orcadas Rise (Figures 1 and 2).

The largest discrepancy between the three mean paths is in the vicinity of Ewing Bank at the end of the Falkland Plateau ($\sim 45^\circ$ W), where our mean path lies ~ 290 km to the south of *Orsi et al.* [1995] and up to 332 km south of *Gille* [1994]. After crossing the north Scotia Ridge our mean path turns sharply eastward following the deep valley between the north Scotia Ridge and the Falkland Plateau, and then northeastward, hugging the southeast flank of Ewing Bank at the eastern end of the Falkland Plateau. The other paths cross the Falkland Plateau before turning eastward. We believe this difference is due to a persistent divergence between the surface and subsurface PF expressions in this region.

Guretskii [1987], working with SST data, also placed the PF consistently to the south and along the southeast flank of Ewing Bank. Several recent studies have placed the subsurface expression of the PF as crossing the Falkland Plateau and flowing eastward along the north side of Ewing Bank [*Peterson and Whitworth*, 1989; *Gille*, 1994; *Orsi et al.*, 1995]. It is in this region that the SAF rejoins the PF. *Peterson and Whitworth* [1989] concluded that the SAF and PF are spaced closely together north of Ewing Bank, at times effectively merging to form one continuous front. The surface expression of the PF was not detectable in their transects apparently lying farther to the south [*Peterson and Whitworth*, 1989]. *Mackintosh* [1946] outlined paths for the PF both north and south of Ewing Bank. Some drifter data also indicate a strong northeastward flow along the southeast flank of Ewing Bank [*Hofmann*, 1985; *Davis et al.*, 1996]. *Deacon* [1933] noted that the subsurface expression was often 160–240 km north of the surface expression in the region east of Ewing Bank. *Guretskii* [1987] concluded that the subsurface expression of the PF was often 1° – 2° latitude north of the surface expression in this region of the South Atlantic. Our results strongly support these observations. It appears that while the subsurface expression of the PF often crosses the Falkland Plateau flowing eastward along the north side of Ewing Bank, the surface expression is typically located south of Ewing Bank. A thin surface layer (~ 100 m) of Subantarctic surface water extends southward over Antarctic surface water in this region [*Deacon*, 1933]. Our mean path is also south of those of *Gille* [1994] and *Orsi et al.* [1995] between $\sim 34^\circ$ and 29° W and west of 85° W. Possibly, these differences are also due to frequent separation of the surface and subsurface expressions of the PF.

The annual mean path was similar for the years 1987 and 1988, with an average N-S separation of 53 km (Figure 3). The largest interannual differences were between 90° and 85° W (mean N-S separation of 159 km). The smallest interannual variation was 65° – 55° W (mean N-S separation < 13 km). Interannual variability was also low between $\sim 80^\circ$ and 75° W and

between $\sim 42^\circ$ and 38° W. The mean path for 1988 was not well defined in the area north of the Scotia Ridge near 45° W where few paths were marked (Figure 3). A mean weekly latitudinal displacement of 30 km ($n = 62$) was calculated in areas where portions of the PF were mapped in 2 sequential weeks. A maximum weekly shift of 177 km was observed. Thus the magnitude of variability at weekly timescales is comparable to interannual variations.

The mean ΔT across the PF for the whole region was 1.7° C. This is slightly less than previous estimates of 1.8° – 2.6° C [*Mackintosh*, 1946], 1.8° – 2.1° C [*Houtman*, 1964], and 1.9° – 2.0° C [*Guretskii*, 1987]. In the region south of Africa a mean ΔT of 1.8° C was reported [*Lutjeharms*, 1985]. Our mean width of 47 km for the PF agrees well with the width of 44 km given by *Gille* [1994] and the 40 km estimate of *Sciremammano et al.* [1980] and is somewhat less than the 61 km distance of *Nowlin and Clifford* [1982]. *Nowlin and Clifford* [1982] noted their width is an overestimate because transects were likely not normal to the flow direction.

One way to quantify the meandering intensity of a strong jet or front is to calculate the spatial root-mean-square (rms) displacement at right angles from the mean path [*Lee and Cornillon*, 1995]. The spatial rms displacement for the whole region over the 2 year period was 100 km. *Gille* [1994] reported typical meander distances of about 75 km to either side of the mean path for the whole Southern Ocean.

If we examine the behavior of the PF by longitudinal bins, it is apparent that there are large regional variations (Figure 4). In Figure 4 the area from 50° to 45° W has been divided into two columns with data from north and south of the north Scotia Ridge (clearly two different domains, see Figures 1 and 2) presented separately.

There is an inverse correlation between meandering intensity (as measured by the spatial rms displacement) and both temperature change and width of the front (Figures 4e, 4f, and 4g). The cross-correlation coefficients for these two relationships were -0.45 and -0.57 , respectively (both significant at the 95% confidence level by Student's t test). The SST gradient across the PF is largest and the cross-frontal distance is widest in the region of low variability between $\sim 60^\circ$ and 55° W (Figures 1, 4f, and 4g). *Gille* [1994] also found evidence for an intensification of the ACC fronts in this area. The very high spatial rms displacement at 25° – 20° W is partly a function of the small number of PF paths marked in this area (Figures 1 and 4e).

The absolute value of the N-S bottom slope was calculated for each point along the mean path of the Polar Front over a distance totaling 90 km (Figure 4d). For the area between 50° and 45° W south of 54° S, bottom slope was calculated in the E-W direction because the PF is moving latitudinally in this area (Figure 4d). Meandering intensity was inversely related to bottom slope (Figures 4d and 4e). The cross-correlation coefficient between Figures 4d and 4e was -0.44 (significant at the 95% confidence level by Student's t test). It can be seen that where the N-S bottom slope is large ($> \sim 8$ m km $^{-1}$), meandering intensity is low (Figures 4d and 4e). Conversely, in areas where the ocean floor is weakly sloped, meandering intensity is elevated.

It is clear that changes in the planetary potential vorticity along the path of the PF are largely a function of ocean depth, despite large latitudinal shifts (Figures 4a, 4b, and 4c). Planetary potential vorticity does not remain constant where the PF crosses large topographic features, including Drake Passage, the north Scotia Ridge, and the Islas Orcadas Rise. Note that

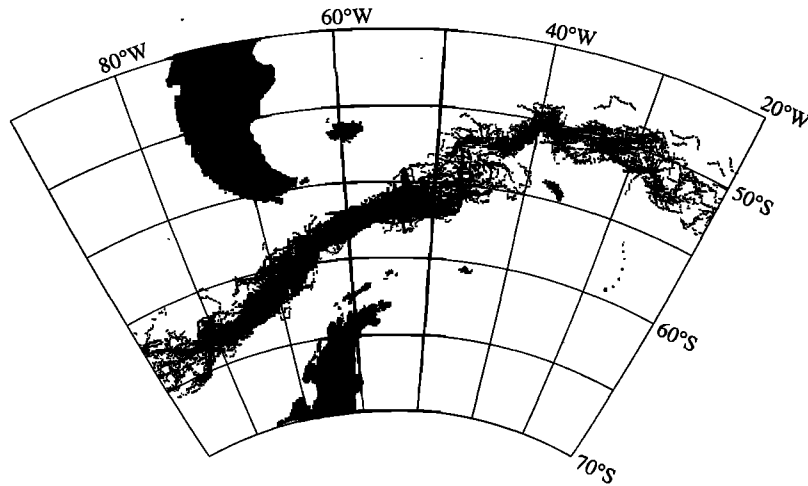


Figure 1. Displayed are all paths for the Antarctic Polar Front digitized for the years 1987–1988.

despite the large latitudinal shifts across the whole region, the mean planetary potential vorticity along the PF is similar in the open ocean areas west of Drake Passage and between $\sim 25^\circ$ and 20°W (Figure 4b).

Insight into the regional variations apparent in Figure 4 can be gained if we compare the mean path of the PF with the planetary potential vorticity field (Plate 2). The mean path can be seen to turn northward at $\sim 83^\circ\text{W}$ when it encounters areas of increasing planetary potential vorticity (shallower depths) west of the Antarctic Peninsula. The PF continues moving equatorward as it is forced across planetary potential vorticity contours through Drake Passage. There is a sharp poleward turn at $40^\circ\text{--}39^\circ\text{W}$, where planetary potential vorticity values decline by $>50\%$ at the eastern end of the Falkland Plateau. The front turns southward as it approaches the Islas Orcadas Rise ($\sim 28^\circ\text{W}$) and turns equatorward again while crossing this feature.

The mean planetary potential vorticity along the mean path of the PF was calculated at each longitude within a moving 2° longitude wide window. In Plate 3 the planetary potential vorticity field and mean PF path from Plate 2 are reproduced, but

along each longitudinal line a relatively narrow range of planetary potential vorticity values, consisting of the calculated mean planetary potential vorticity value of $\pm 10^{-9} \text{ m}^{-1} \text{ s}^{-1}$, has been set to white. This narrow range of planetary potential vorticity values can be considered as encompassing a local region of quasi-uniform planetary potential vorticity (the mean value of $\pm \sim 5\%$). The PF is free to meander within this region while maintaining a relatively constant planetary potential vorticity. Comparing Figure 1 and Plates 2 and 3, it can be seen that although mean planetary potential vorticity along the PF changes drastically through this whole region, locally the PF tends to follow lines of relatively constant planetary potential vorticity. Thus the envelope of PF paths tends to correspond to the size of the local region of quasi-uniform planetary potential vorticity (compare Figure 1 and Plate 3).

This relationship between gradients in planetary potential vorticity and path variability is especially clear west of Drake Passage. In Figure 1 the envelope of PF paths is widest west of $\sim 83^\circ\text{W}$, where the weak bottom slope results in a relatively broad area of quasi-uniform planetary potential vorticity (Figure 1 and Plate 3). The envelope of PF paths narrows consid-

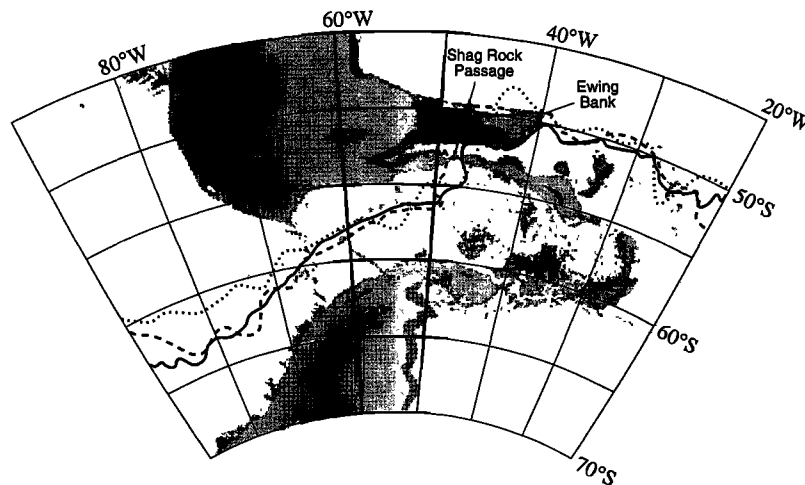


Figure 2. The mean path for the Antarctic Polar Front (PF) is shown (solid line). Also shown for comparison are the PF paths from Orsi *et al.* [1995] (dashed line) and from Gille [1994] (dotted line). Bathymetric contours show areas shallower than 2000 m (light grey) and areas shallower than 3000 m (dark grey).

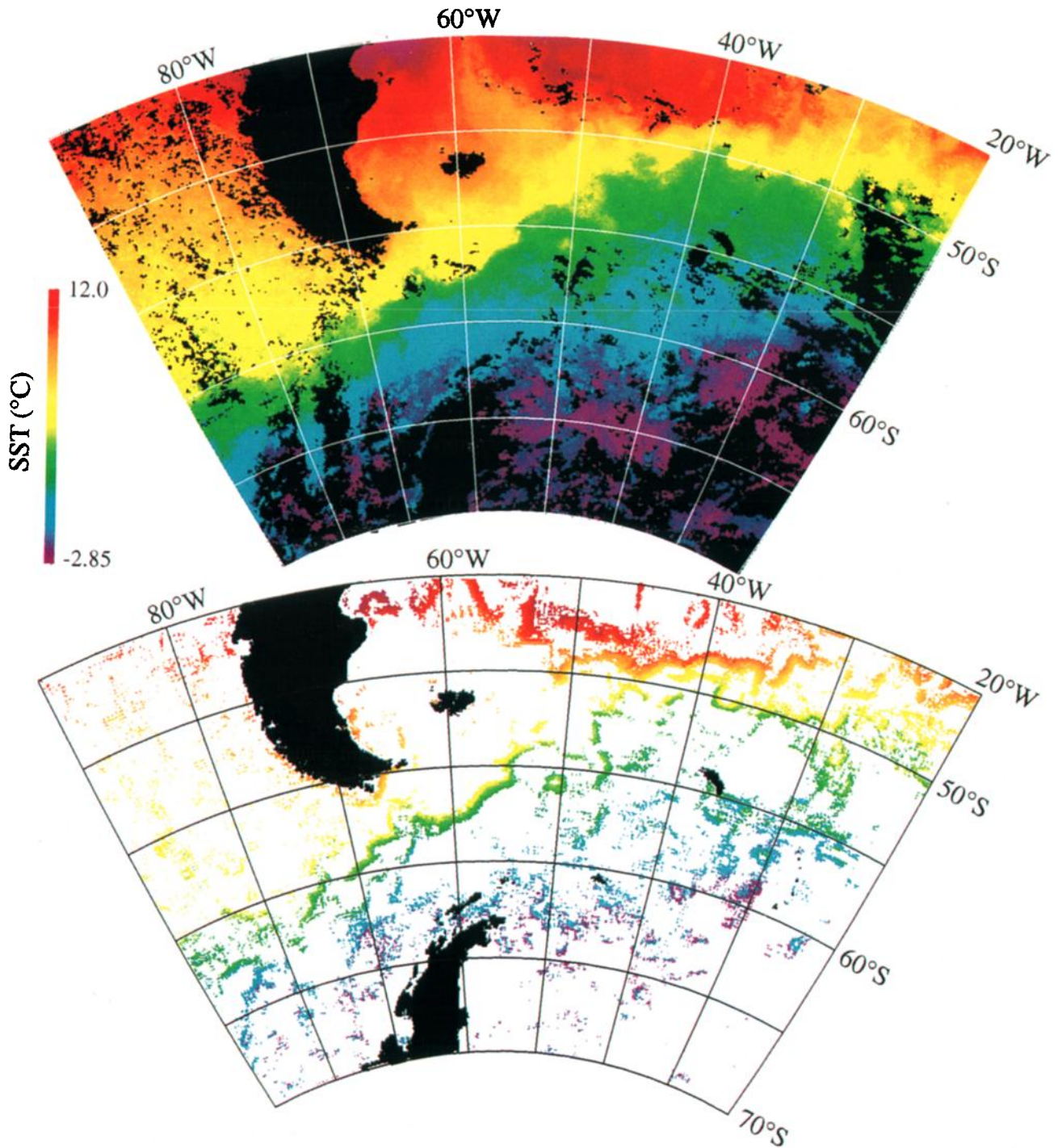


Plate 1. (top) Mean sea surface temperature from the first week of 1987. Areas in black had no valid sea surface temperature (SST) data during the week. (bottom) The gradient map is a subset of the SST image where only pixels within strong SST gradients have been retained (see text for details). The Antarctic Polar Front can be seen stretching from SW to NE across the Scotia Sea. Farther north are strong gradients associated with the Subantarctic Front.

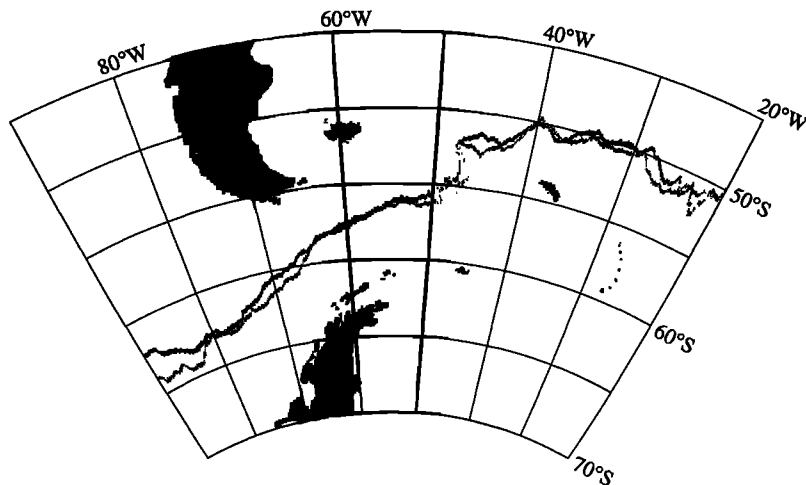


Figure 3. The mean path of the Antarctic Polar Front for the years 1987 (black line) and 1988 (grey line) are shown. The annual paths are not well defined in the highly variable northern Scotia Sea and east of $\sim 25^\circ\text{W}$, where few paths were marked.

erably between $\sim 78^\circ$ and 76°W , where an increase in the bottom slope causes larger gradients in the planetary potential vorticity field. The envelope of PF paths broadens again as Drake Passage is approached and the local region of quasi-uniform planetary potential vorticity expands (Figure 1 and Plate 3). At $\sim 54^\circ\text{W}$ the PF crosses several narrow valleys and enters another relatively broad, flat region of quasi-uniform planetary potential vorticity, where meandering intensity increases considerably (Figures 1 and 4e and Plate 3). After crossing the north Scotia Ridge the PF can be seen to follow relatively constant planetary potential vorticity lines along the Falkland Plateau. Between 35° and 30°W and east of $\sim 24^\circ\text{W}$ the region of quasi-uniform planetary potential vorticity broadens again, as does the envelope of PF paths (compare Figure 1 and Plate 3).

In general, variability in the front's position is higher as it passes through areas with a relatively flat bottom (west of $\sim 83^\circ\text{W}$, east of $\sim 33^\circ\text{W}$, and in the northern Scotia Sea), and variability is lower where steep bottom slopes result in strong gradients in the planetary potential vorticity field (within Drake Passage, $\sim 78^\circ$ – 76°W and along the Falkland Plateau, compare Figures 1 and 4e and Plate 3).

The lowest variability in the PF's position at weekly and interannual timescales is in the region between 65° and 55°W (Figures 3 and 4e). We believe the local bathymetry plays a crucial role in stabilizing the position of the PF here (Plate 4). Again, a narrow range of planetary potential vorticity values consisting of the running mean of planetary potential vorticity along the mean PF path ($\pm \sim 5\%$) has been set white along each line of longitude. It can be seen that in this region the PF closely follows several deep, narrow (< 50 km wide) valleys, which are likely associated with spreading centers. The PF appears to follow local planetary potential vorticity contours where possible. The seamounts north and south of the valley at $\sim 62^\circ$ – 57°W cause contours of planetary potential vorticity to be pinched tightly together, inhibiting lateral motions of the PF (Plate 4). The spatial rms between 62° and 57°W was 43 km over the 1987–1988 period. Mean N-S bottom slope between 62° and 57°W was 10.8 m km^{-1} . Interannual variability was also low with a mean latitudinal difference of 18 km (Figure 3). The PF crosses and then leaves the valley where it narrows at

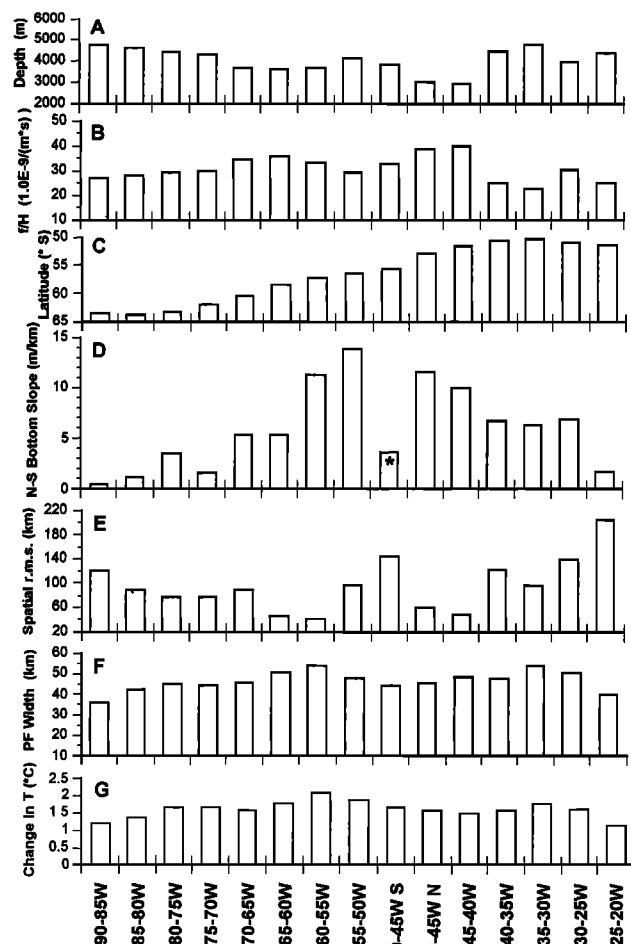


Figure 4. Statistical properties of the Antarctic Polar Front (90° – 20°W) averaged into 5° longitudinal bins are displayed. (a) The depth along the mean path of the PF, (b) planetary potential vorticity (f/H) along the mean path, (c) latitude, (d) N-S bottom slope (asterisk denotes where E-W slope is shown), (e) spatial rms variation from the mean path, (f) width of the PF, and (g) the change in temperature across the PF.

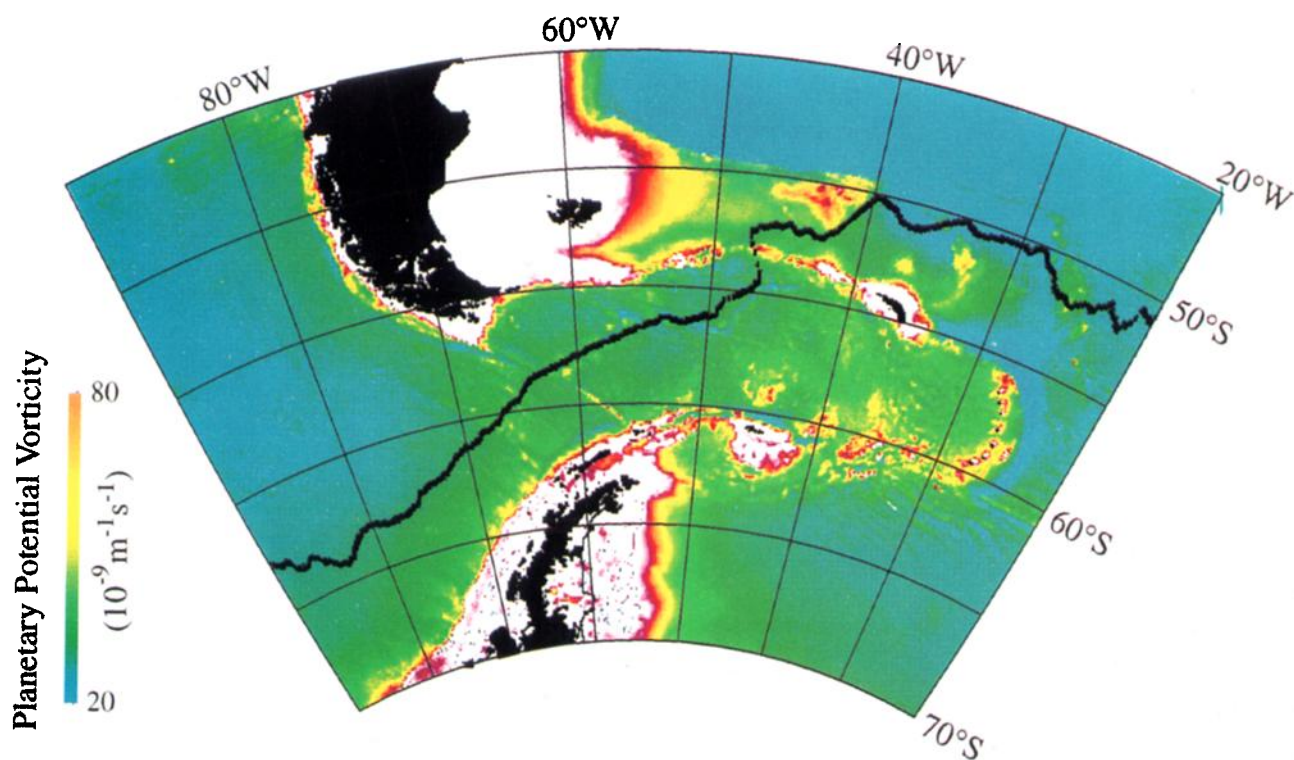


Plate 2. The mean path of the Antarctic Polar Front is overlain on a map of planetary potential vorticity (f/H), where f is the Coriolis parameter and H is ocean depth. The predicted bathymetry data was remapped to have the same resolution as the SST data for this figure.

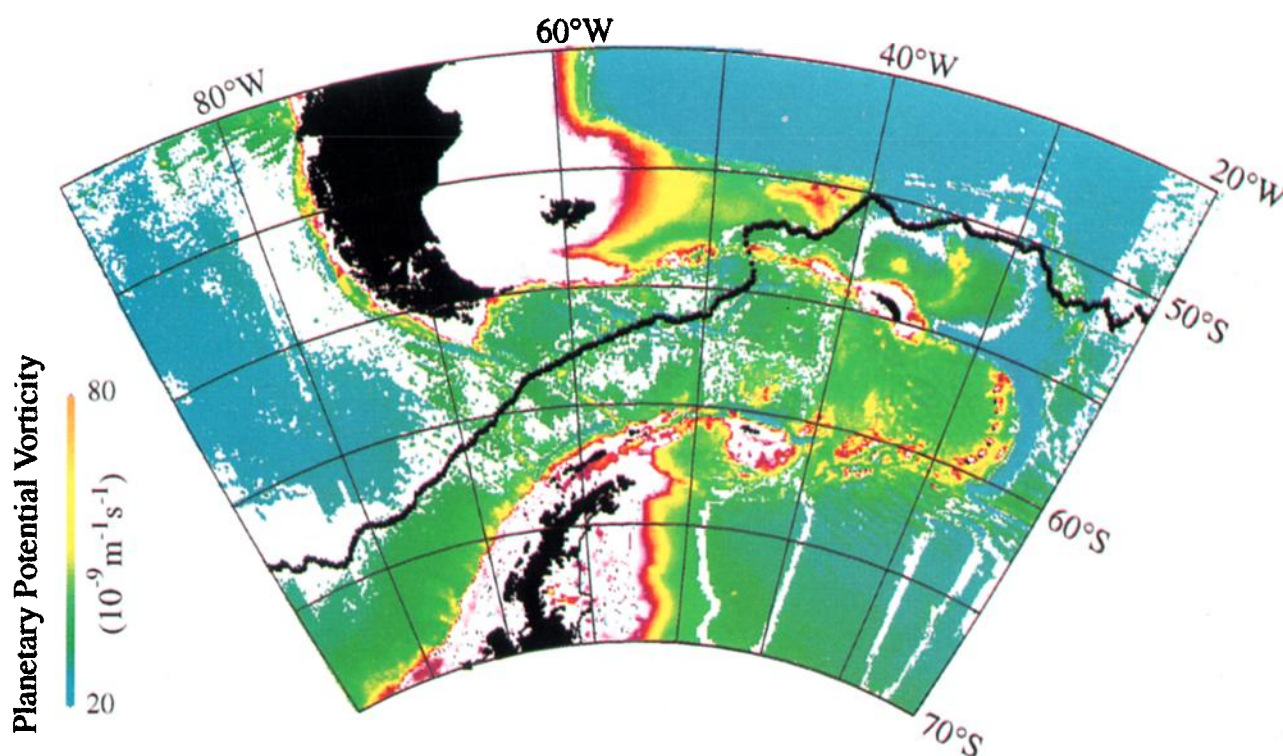


Plate 3. Mean path of the Polar Front overlain on a map of planetary potential vorticity (f/H). The mean planetary potential vorticity along the PF was calculated at each longitude from points within a moving 2° longitude wide window. A range of planetary potential vorticity values consisting of the mean value $\pm 10^{-9} \text{ m}^{-1} \text{ s}^{-1}$ along each line of longitude has been set white. The predicted bathymetry data was remapped to the same resolution as the SST data.

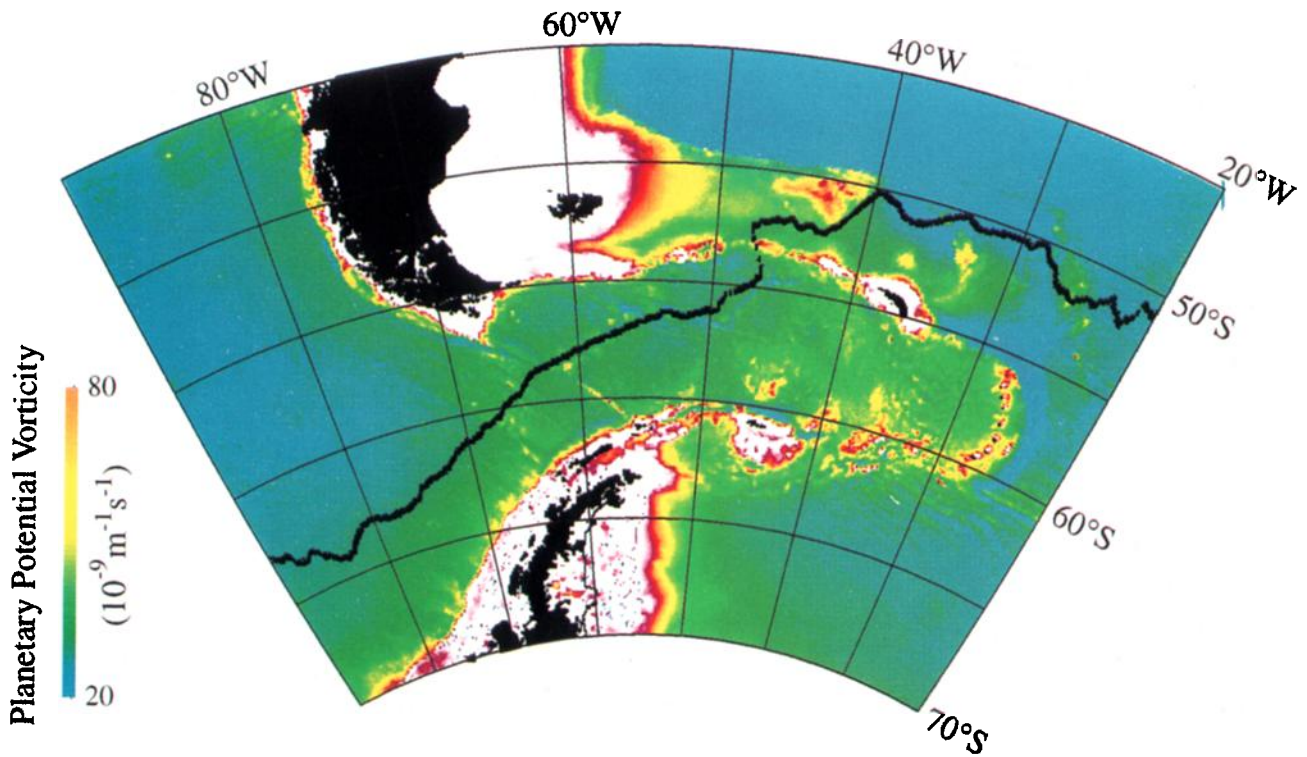


Plate 2. The mean path of the Antarctic Polar Front is overlain on a map of planetary potential vorticity (f/H), where f is the Coriolis parameter and H is ocean depth. The predicted bathymetry data was remapped to have the same resolution as the SST data for this figure.

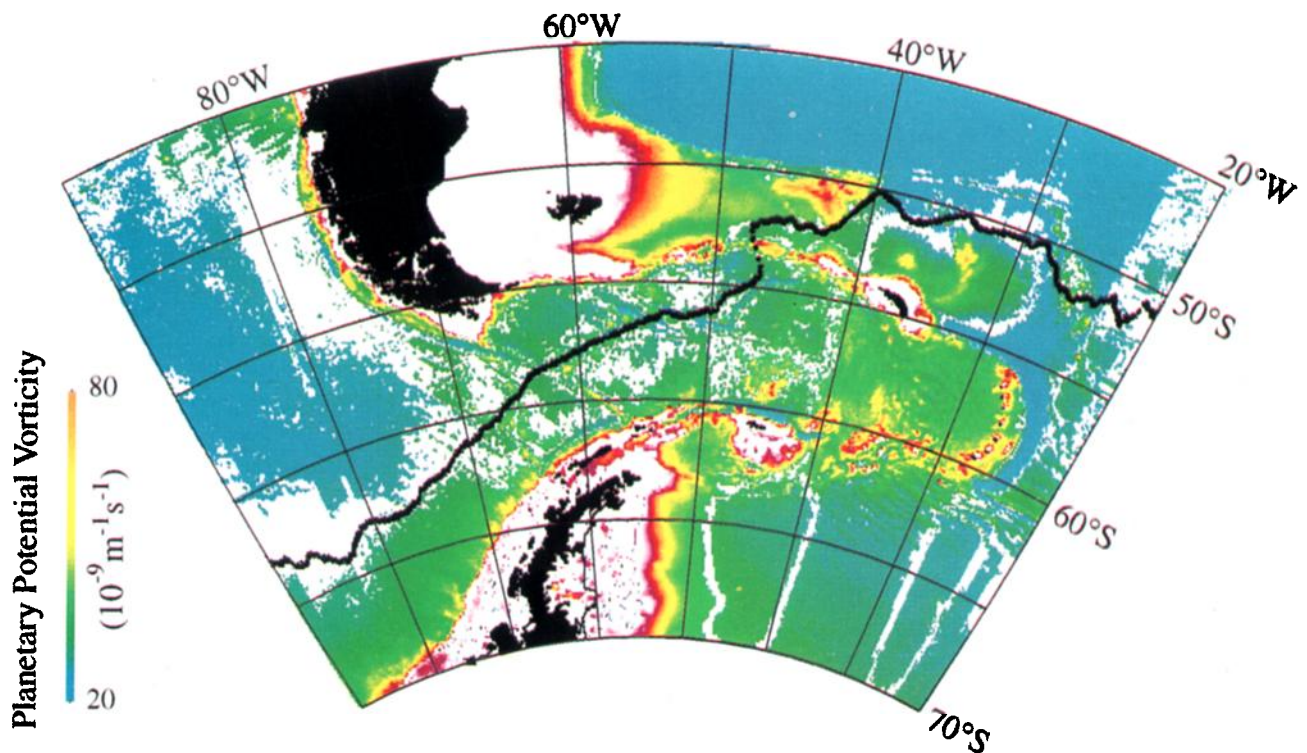


Plate 3. Mean path of the Polar Front overlain on a map of planetary potential vorticity (f/H). The mean planetary potential vorticity along the PF was calculated at each longitude from points within a moving 2° longitude wide window. A range of planetary potential vorticity values consisting of the mean value $\pm 10^{-9} \text{ m}^{-1} \text{ s}^{-1}$ along each line of longitude has been set white. The predicted bathymetry data was remapped to the same resolution as the SST data.

References

- Bishop, J. K. B., and W. B. Rossow, Spatial and temporal variability of global surface solar irradiance, *J. Geophys. Res.*, **96**, 16839–16858, 1991.
- Brown, J. W., O. B. Brown, and R. H. Evans, Calibration of advanced very high resolution radiometer infrared channels: A new approach to nonlinear correction, *J. Geophys. Res.*, **98**, 18257–18268, 1993.
- Chelton, D. B., M. G. Schlax, D. L. Witter, and J. G. Richman, Geosat altimeter observations of the surface circulation of the Southern Ocean, *J. Geophys. Res.*, **95**, 17877–17903, 1990.
- Cornillon, P., The effect of the New England seamounts on Gulf Stream meandering as observed from satellite IR imagery, *J. Phys. Oceanogr.*, **16**, 386–389, 1986.
- Daniault, N., and Y. Ménard, Eddy kinetic energy distribution in the Southern Ocean from altimetry and FGGE drifting buoys, *J. Geophys. Res.*, **90**, 11877–11889, 1985.
- Davis, R. E., P. D. Killworth, and J. R. Blundell, Comparison of Autonomous Lagrangian Circulation Explorer and fine resolution Antarctic model results in the South Atlantic, *J. Geophys. Res.*, **101**, 855–884, 1996.
- Deacon, G. E. R., A general account of the hydrology of the South Atlantic ocean, *Discovery Rep.*, **VII**, 177–238, 1933.
- Deacon, G. E. R., The hydrology of the Southern Ocean, *Discovery Rep.*, **XV**, 1–124, 1937.
- Fu, L. L., and D. B. Chelton, Temporal variability of the Antarctic circumpolar current observed from satellite altimetry, *Science*, **226**, 343–346, 1984.
- Gille, S. T., Mean sea surface height of the Antarctic Circumpolar Current from Geosat data: Method and application, *J. Geophys. Res.*, **99**, 18255–18273, 1994.
- Gille, S. T., and K. A. Kelly, Scales of spatial and temporal variability in the Southern Ocean, *J. Geophys. Res.*, **101**, 8759–8773, 1996.
- Gordon, A. L., D. T. Georgi, and H. W. Taylor, Antarctic Polar Front Zone in the western Scotia Sea—Summer 1975, *J. Phys. Oceanogr.*, **7**, 309–328, 1977.
- Gordon, A. L., E. Molinelli, and T. Baker, Large-scale dynamic topography of the Southern Ocean, *J. Geophys. Res.*, **83**, 3023–3032, 1978.
- Grose, T. J., J. A. Johnson, and G. R. Bigg, A comparison between the FRAM (Fine Resolution Antarctic Model) results and observations in the Drake Passage, *Deep Sea Res., Part I*, **42**, 365–388, 1995.
- Guretskii, V. V., Surface thermal fronts in the Atlantic sector of the Southern Ocean, *Sov. Meteorol. Hydrol.*, Engl. Transl., **8**, 67–73, 1987.
- Hansen, D. V., and G. A. Maul, A note of the use of sea surface temperature for observing ocean currents, *Remote Sens. Environ.*, **1**, 161–164, 1970.
- Hofmann, E. E., The large-scale horizontal structure of the Antarctic Circumpolar Current from FGGE drifters, *J. Geophys. Res.*, **90**, 7087–7097, 1985.
- Hofmann, E. E., and T. Whitworth III, A synoptic description of the flow at Drake Passage from year-long measurements, *J. Geophys. Res.*, **90**, 7177–7187, 1985.
- Houtman, T. J., Surface temperature gradients at the Antarctic Convergence, *N. Z. J. Geol. Geophys.*, **7**, 245–270, 1964.
- Ikeda, Y., G. Siedler, and M. Zwierz, On the variability of Southern Ocean Front locations between southern Brazil and the Antarctic Peninsula, *J. Geophys. Res.*, **94**, 4757–4762, 1989.
- Johnson, M. A., Southern Ocean surface characteristics from FGGE buoys, *J. Phys. Oceanogr.*, **19**, 696–705, 1989.
- Joyce, T. M., W. Zenk, and J. M. Toole, The anatomy of the Antarctic Polar Front in the Drake Passage, *J. Geophys. Res.*, **83**, 6093–6113, 1978.
- Koblinsky, C. J., The global distribution of f/H and the barotropic response of the ocean, *J. Geophys. Res.*, **95**, 3213–3218, 1990.
- Lee, T., and P. Cornillon, Temporal variation of meandering intensity and domain-wide lateral oscillations of the Gulf Stream, *J. Geophys. Res.*, **100**, 13603–13613, 1995.
- Legeckis, R., Oceanic Polar Front in the Drake Passage—Satellite observations during 1976, *Deep Sea Res.*, **24**, 701–704, 1977.
- Lutjeharms, J. R. E., Location of frontal systems between Africa and Antarctica: Some preliminary results, *Deep Sea Res., Part A*, **32**, 1499–1509, 1985.
- Lutjeharms, J. R. E., and H. R. Valentine, Southern Ocean thermal fronts south of Africa, *Deep Sea Res., Part A*, **31**, 1461–1475, 1984.
- Mackintosh, N. A., The Antarctic Convergence and the distribution of surface temperatures in Antarctic waters, *Discovery Rep.*, **XXIII**, 177–212, 1946.
- Nowlin, W. D., Jr., and M. Clifford, The kinematic and thermohaline zonation of the Antarctic Circumpolar Current at Drake Passage, *J. Mar. Res.*, **40**, suppl., 481–507, 1982.
- Nowlin, W. D., Jr., and J. M. Klinck, The physics of the Antarctic Circumpolar Current, *Rev. Geophys.*, **24**, 469–491, 1986.
- Olson, D. B., O. B. Brown, and S. R. Emmerson, Gulf Stream frontal statistics from Florida Straits to Cape Hatteras derived from satellite and historical data, *J. Geophys. Res.*, **88**, 4569–4577, 1983.
- Orsi, A. H., T. Whitworth III, and W. D. Nowlin Jr., On the meridional extent and fronts of the Antarctic Circumpolar Current, *Deep Sea Res., Part I*, **42**, 641–673, 1995.
- Peterson, R. G., and T. Whitworth III, The Subantarctic and Polar Fronts in relation to deep water masses through the southwestern Atlantic, *J. Geophys. Res.*, **94**, 10817–10838, 1989.
- Sandwell, D. T., and B. Zhang, Global mesoscale variability from the Geosat Exact Repeat mission: Correlation with ocean depth, *J. Geophys. Res.*, **94**, 17971–17984, 1989.
- Sciremammano F., Jr., R. D. Pillsbury, W. D. Nowlin Jr., and T. Whitworth III, Spatial scales of temperature and flow in Drake Passage, *J. Geophys. Res.*, **85**, 4015–4028, 1980.
- Smith, E., J. Vasquez, A. Tran, and R. Sumagaysay, Satellite-derived sea surface temperature data available from the NOAA/NASA Pathfinder program, *Eos Trans. AGU Electron. Suppl.*, April 2, 1996. (Available as http://www.agu.org/eos_elec/95274e.html)
- Smith, W. H. F., and D. T. Sandwell, Bathymetric prediction from dense satellite altimetry and sparse shipboard bathymetry, *J. Geophys. Res.*, **99**, 21803–21824, 1994.
- Sparrow, M. D., K. J. Heywood, J. Brown, and D. P. Stevens, Current structure of the south Indian Ocean, *J. Geophys. Res.*, **101**, 6377–6391, 1996.

M. R. Abbott, J. K. Moore, and J. G. Richman, College of Oceanic and Atmospheric Sciences, Oregon State University, 104 Ocean Administration Building, Corvallis, OR 97331-5503. (e-mail: mark@oce.orst.edu;jmoore@oce.orst.edu;jrichman@oce.orst.edu)

(Received February 5, 1997; revised May 27, 1997; accepted June 4, 1997.)